JACS
JOURNAL OF THE AMERICAN CHEMICAL SOCIETY
Article
pubs.acs.org/JACS

Following the Reduction of Oxygen on TiO_2 Anatase (101) Step by Step

Martin Setvin,*[,†] Ulrich Aschauer,[‡] Jan Hulva,[†] Thomas Simschitz,[†] Benjamin Daniel,[†] Michael Schmid,[†] Annabella Selloni,[§] and Ulrike Diebold[†]

[†]TU Wien, Wiedner Hauptstrasse 8-10/134, 1040 Vienna, Austria
[‡]Department of Chemistry and Biochemistry, University of Bern, Freiestrasse 3, 3012 Bern, Switzerland
[§]Department of Chemistry, Frick Laboratory, Princeton University, Princeton, New Jersey 08544, United States

Supporting Information

ABSTRACT: We have investigated the reaction between O_2 and H_2O, coadsorbed on the (101) surface of a reduced TiO_2 anatase single crystal by scanning tunneling microscopy, density functional theory, temperature-programmed desorption, and X-ray photoelectron spectroscopy. While water adsorbs molecularly on the anatase (101) surface, the reaction with O_2 results in water dissociation and formation of terminal OH groups. We show that these terminal OHs are the final and stable reaction product on reduced anatase. We identify OOH as a metastable intermediate in the reaction. The water dissociation reaction runs as long as the surface can transfer enough electrons to the adsorbed species; the energy balance and activation barriers for the individual reaction steps are discussed, depending on the number of electrons available. Our results indicate that the presence of donor dopants can significantly reduce activation barriers for oxygen reduction on anatase.

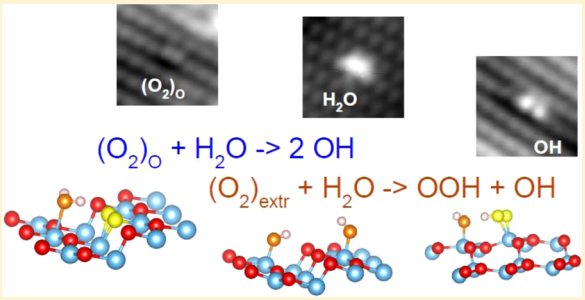

INTRODUCTION

TiO_2 is a prototypical metal oxide used in catalytic and photocatalytic reactions.[1−3] The surface chemistry of oxygen and water builds the base for important processes such as photocatalytic water oxidation[4−6] and the oxygen reduction reaction (ORR),[7] which are essentially inverse reactions mediated by holes and electrons, respectively.[5] Water oxidation is a hole-mediated, multistep process

$$2H_2O + 4h^+ \rightarrow O_2 + 4H^+ \quad (1)$$

while the ORR is based on activating molecular oxygen by electron transfer from the substrate and subsequent reactions with coadsorbed water:[8]

$$O_2 + e^- \rightarrow (O_2)^- \quad (2)$$

$$(O_2)^- + H_2O + e^- \rightarrow OOH^- + OH^- \quad (3)$$

$$OOH^- + e^- \rightarrow (O_{ad})^- + OH^- \quad (4)$$

$$(O_{ad})^- + H_2O + e^- \rightarrow 2OH^- \quad (5)$$

$$OOH^- + H_2O \rightarrow H_2O_2 + OH^- \quad (6)$$

$$H_2O_2 + 2e^- \rightarrow 2OH^- \quad (7)$$

Water oxidation and the ORR involve the same intermediate species, namely, OH, OOH, or H_2O_2. While the pathway through OOH dissociation (eqs 3−5) is reported more often than the alternative scenario involving H_2O_2 (eqs 6−7), the exact reaction pathways are still a matter of an intense debate.[9] Identification of reaction intermediates is difficult because they are often short-lived and thus present in minute quantities. Obtaining molecular-scale insights into the reaction between water and activated O_2 is a key for understanding photocatalytic processes in real environments.

Here we use a combination of scanning tunneling microscopy (STM) and density functional theory (DFT) to follow the reactions between water and oxygen on the anatase TiO_2(101) surface. Information obtained by these two techniques is supported by temperature-programmed desorption (TPD) and X-ray photoelectron spectroscopy (XPS). All experiments were performed on a reduced (electron-rich) sample, which provides the electrons required for the ORR. We show that the reaction between H_2O and O_2 results in water dissociation and formation of terminal OH groups, which are the only and final reaction product, stable at room temperature (RT). We also identify OOH as a metastable reaction intermediate, which decomposes slightly below room temperature. The experimental data indicate that H_2O_2 can also form during the reaction, but is very unstable in the presence of excess electrons and spontaneously decomposes into a pair of terminal $(OH)^-$ groups.

Received: April 26, 2016
Published: July 3, 2016

DOI: 10.1021/jacs.6b04004
J. Am. Chem. Soc. 2016, 138, 9565−9571

The reactions between oxygen and water have been previously investigated in detail on the prototypical rutile TiO_2(110) surface;[10,11] here, we show that the pathway for anatase is significantly different. On rutile (110), adsorbed water reacts with surface oxygen vacancies (which are not present on the anatase (101) surface),[12,13] forming bridging hydroxyl groups.[14] The bridging hydroxyls react with adsorbed O_2 and result in many metastable adsorbed species such as terminal OH groups, H_2O_2, OOH, and H_3O_2.[11] However, all these species are unstable at room temperature and desorb as H_2O.[10] The rutile (110) surface was reported to contain exclusively bridging OH groups after such a reaction cascade.[11,15]

EXPERIMENTAL AND THEORETICAL METHODS

STM measurements were performed at T = 6 K in a UHV chamber with a base pressure below 1 × 10^{-11} mbar, equipped with a commercial Omicron LT-STM head. To slow down any thermally induced reactions, and render reaction products observable, we have performed the experiments at liquid-He temperatures. At low temperature, imaging conditions are also more stable in STM. Controlled low-temperature annealing of the sample was performed in a manipulator cooled by flowing nitrogen gas. The temperature was measured by a K-type thermocouple attached to the sample holder. We estimate that the quoted temperatures are accurate within ±10 K. Electrochemically etched W STM tips were cleaned by Ar^+ sputtering and treated on a Au(110) surface to obtain a reproducible, metallic tip condition. We used a single-crystalline mineral anatase TiO_2(101) sample, naturally doped by 1% Nb.[16] The surface was prepared by ex-situ cleaving or polishing (both types were used) and subsequent cleaning in vacuum by cycles of Ar^+ sputtering (1 keV) and annealing to 950 K.[17]

The TPD measurements were performed in a separate UHV system with a base pressure of 5 × 10^{-11} mbar using a HIDEN quadrupole mass spectrometer in a line-of-sight configuration. Here the anatase sample was mounted on a Ta back plate, cooled by a Janis ST-400 UHV liquid-He flow cryostat, and heated by direct current through the back plate. The temperature was measured by a K-type thermocouple spot-welded to the sample plate, and calibrated using multilayer desorption of several gases (O_2, H_2O, CO). The resulting uncertainty in the absolute temperature reading is estimated to be ±3 K (increasing up to ±10 K at temperatures below ∼40 K). During the TPD measurements, the sample was biased at −100 V to prevent electrons from the quadrupole's filament reaching the sample surface. Gases were dosed by an effusive molecular beam with a hat-shaped profile.[18] This produces a beam spot of ≈3.5 mm diameter at the sample (sample size 4 × 6 mm^2). Thus, only the TiO_2(101) surface is exposed to the molecular beam. The dose rate under these conditions is approximately 1.2 ML/min. For the TPD measurements a linear temperature ramp of 1 K/s was used.

XPS spectra were measured in the same vacuum system with a hemispherical electrostatic energy analyzer (SPECS Phoibos 150), using a monochromatized Al Kα X-ray source (SPECS Focus 500). Data were recorded at a sample temperature of T = 34 K. Any influence of the X-rays and contamination from the residual gas were carefully checked by TPD spectra recorded after the XPS data were taken; no radiation-induced damage was observed. XPS was measured under a 60° exit angle off normal.

Spin-polarized DFT calculations were performed using the Perdew–Burke–Ernzerhof (PBE)[19] exchange-correlation functional as implemented in the QUANTUM Espresso package.[20] We used ultrasoft pseudopotentials[21] with Ti(3s, 3p, 3d, 4s), Nb(4s, 4p, 4d, 5s), O(2s, 2p), and H(1s) states in the valence. Wave functions were expanded in plane waves with a maximum kinetic energy of 25 Ry, while using a cutoff of 200 Ry for the augmented density. We applied a Hubbard U term[22] of 3.5 eV to both Ti 3d and Nb 4d states. This computational approach has been used extensively to describe excess electrons in anatase TiO_2.[23] Nudged elastic band (NEB) calculations were performed using the climbing image method,[24] and structures and pathways were relaxed until forces converged below 0.05 eV/Å. For all calculations we used a slab with a 10.262 × 11.310 $Å^2$ surface supercell ([3, 0] × [1, 2] with regard to the DFT-relaxed primitive cell of the anatase (101) surface), 3 TiO_2 layers, and a 10.5 Å vacuum gap separating periodic images along the surface normal direction. Due to the large cell size, reciprocal-space sampling was restricted to the Γ point. The bottom-most atoms were kept fixed to mimic the presence of bulk. Dipole corrections were found to have a negligible effect on the energetics (see Supporting Information Table ST1), and thus were not included in our standard setup.

RESULTS

When oxygen and water are codosed on the anatase (101) surface at low temperature, isolated water molecules and isolated oxygen-related species are clearly identified, see Figure 1a. We note that a reliable procedure for identifying these species in STM images was described in ref 25. After such a surface was annealed to room temperature, most of the original molecules have disappeared, and a new species is dominant, indicating that a reaction between water and oxygen has occurred (Figure 1b). In the following, we show that the resulting species are terminal OH groups. They exhibit a surprisingly high stability, and are present even after annealing above 400 K (see Supporting Information Figure SF1).

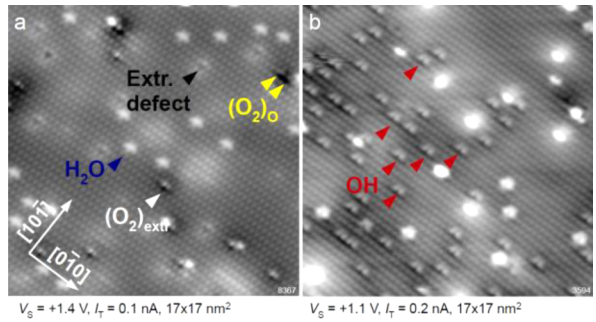

Figure 1. (a) STM image of the anatase (101) surface after codosing O_2 and H_2O at T = 105 K (imaged at T = 6 K). (b) The surface after annealing to room temperature for 10 min.

Water adsorbs molecularly on the anatase (101) surface with an adsorption energy of ∼0.75 eV and desorbs below room temperature[26,27] (see Supporting Information Figure SF2). Oxygen adsorption is a more complicated process with multiple adsorption configurations.[16,28] O_2 can adsorb molecularly in the vicinity of extrinsic defects (marked in Figure 1a), such as the Nb impurity atoms present in our natural anatase sample. These configurations are referred to as $(O_2)_{extr}$. When O_2 is dissociated, the resulting O adatoms are unstable. They immediately incorporate in the surface layer, forming the so-called $(O_2)_O$ species, i.e., a bridging O_2 molecule replacing a surface lattice oxygen atom O_s (see Figure 3a, below). This is the most stable adsorption configuration for adsorbed O. Finally, O_2 readily adsorbs at steps of anatase (101).[28]

While Figure 1b clearly shows a single reaction product, the number of possible reaction pathways is large due to the variety of possible O_2 adsorption configurations. Further, O_2 molecules are distributed unevenly on the surface, depending on the local concentration of defects and steps. To identify unequivocally the reaction product as the terminal OH groups, we performed an experiment focusing on the reaction step

$$(O_2)_O + H_2O \rightarrow 2OH + O_s \quad (8)$$

DOI: 10.1021/jacs.6b04004
J. Am. Chem. Soc. 2016, 138, 9565–9571

which has key importance in the ORR reaction cascade. The anatase surface was cooled to 105 K and bombarded by energetic electrons (Figure 2a), resulting in the creation of surface oxygen vacancies.[12,13] Exposing such a surface to molecular oxygen leads to the formation of $(O_2)_O$ species in a well-defined concentration, see Figure 2b. We note that a similar experiment was shown in ref 16. The reactivity of $(O_2)_O$ toward water was probed by dosing 0.6 Langmuir (L) of H_2O and subsequent annealing to room temperature. The resulting surface is shown in Figure 2c and exhibits species identical to those in Figure 1b. The controlled initial concentration of $(O_2)_O$ allows a statistical analysis of the data. The experiment shown in Figure 2 was repeated three times. The ratio between the final concentration of terminal OH groups and the initial concentration of adsorbed oxygen is 1.9 ± 0.3, in excellent agreement with the stoichiometry of eq 8. We note that any excess water present at the surface desorbs after annealing to RT, and the only remaining species are the terminal OH groups originating from the reaction mechanism in eq 8.

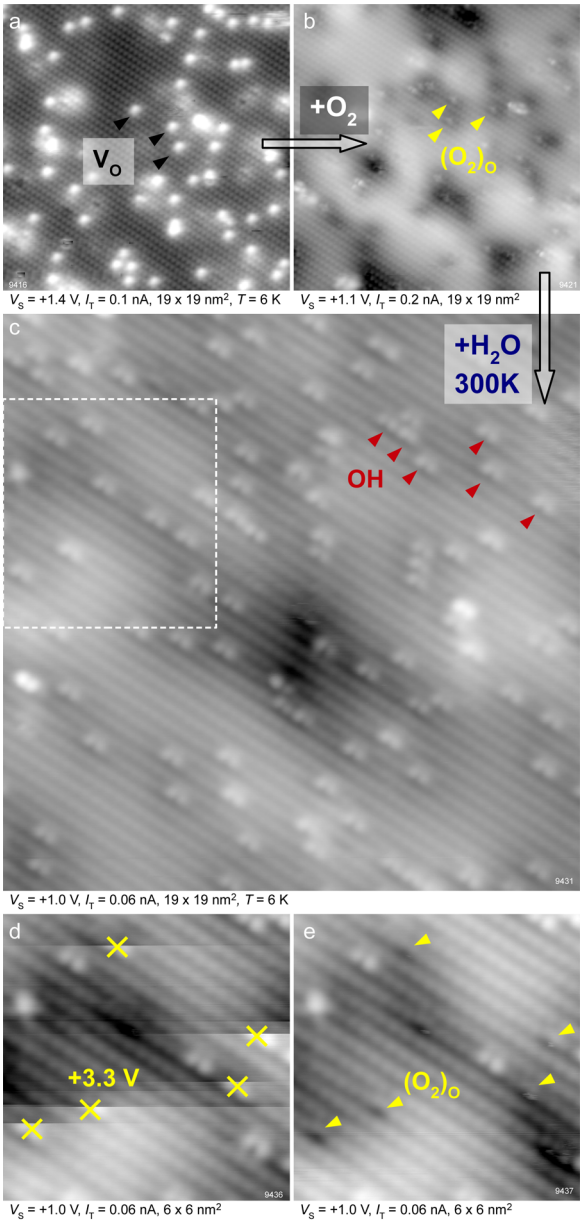

Figure 2. Forming terminal OH groups via a well-defined reaction pathway. (a) Surface V_O's were prepared by electron bombardment of the surface at T = 105 K. (b) The surface from panel a after exposure to 0.6 L O_2 at T = 110 K. (c) Additional dosing of 0.6 L H_2O and annealing to 300 K for 10 min results in the formation of terminal OH groups. (d) Area marked in panel c; × symbols mark positions where voltage pulses were applied (+3.5 V, 0.1 nA). This removes hydrogen from the OH group and leaves $(O_2)_O$, see panel e.

To further confirm the nature of the terminal OH groups, we performed tip-induced manipulation as shown in Figure 2d,e. When the tip is positioned above the OH group and the sample bias is increased to +3.5 V, hydrogen desorbs from the OH,[25,29] leaving only an O atom at the surface. This extra O incorporates into the surface and forms the $(O_2)_O$ species, as shown in Figure 2e.

When scanning at temperatures above ~200 K, adsorbed H_2O molecules start to diffuse, and the reaction of $(O_2)_O$ with water can be observed directly (see Supporting Information Movies SM1 and SM2 and their description in the Supporting Information text). The movies show several details, which are in line with previous studies on TiO_2 rutile.[11,15] In particular, the following apply: (i) there is a weak attractive coupling between the terminal OH and H_2O; (ii) OH groups do not diffuse at the temperature of 200 K, although their mobility is enhanced by the presence of undissociated H_2O molecules, presumably via a proton exchange mechanism between OH and H_2O.[30]

We performed nudged elastic band (NEB)[24] DFT calculations to obtain more detailed information on the reaction mechanisms involved. The computed pathway for reaction 8 [$(O_2)_O$ with H_2O] is shown in Figure 3. The H_2O molecule first adsorbs close to the $(O_2)_O$ dimer, in a position

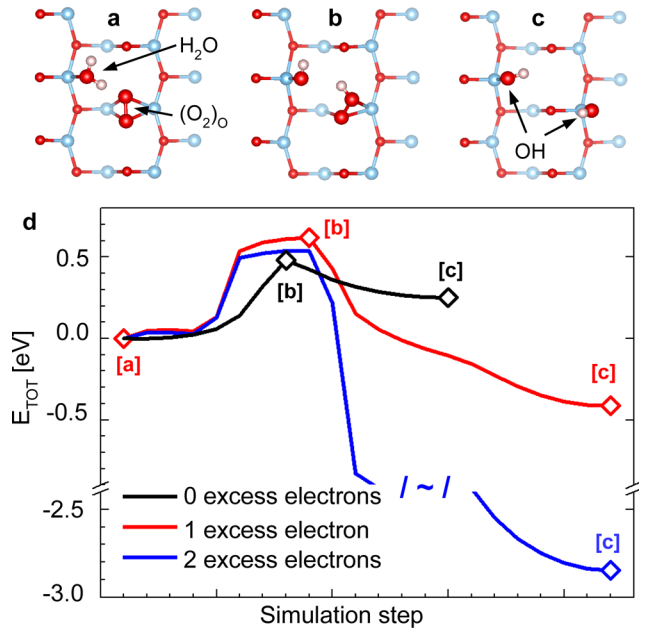

Figure 3. Calculated NEB pathway for the reaction of H_2O with $(O_2)_O$. (a) H_2O adsorbs near the $(O_2)_O$, forming a hydrogen bond. (b) One hydrogen is transferred to the $(O_2)_O$. (c) Relaxation into a pair of terminal OH groups. (d) Energy profile of the reaction for 0, 1, and 2 excess electrons in the slab. Positions corresponding to snapshots a–c are marked in the energy profile. The black line in panel d is shorter because a smaller number of images was used in the corresponding NEB calculation.

DOI: 10.1021/jacs.6b04004
J. Am. Chem. Soc. 2016, 138, 9565–9571

where a hydrogen bond is established between the two species, Figure 3a. One hydrogen atom is then transferred to the $(O_2)_O$ (Figure 3b), and the system spontaneously relaxes into a pair of terminal OH groups (Figure 3c). The corresponding energy profile is shown in Figure 3d. The calculation was performed with different numbers of excess electrons in the system (provided by adsorbed hydrogen atoms on the bottom surface of the slab; see Supporting Information Figure SF3 for energy levels).[31] On a stoichiometric surface the reaction is endothermic by 0.25 eV. Adding 1 electron makes the reaction exothermic, with an energy gain of 0.4 eV. Two excess electrons in the slab result in a large energy gain of 2.6 eV, which can be attributed to the stabilization of the terminal OH groups as negatively charged $(OH)^-$ species. The activation barriers for the hydrogen transfer are comparable in all three cases, from 0.45 to 0.6 eV. The calculated energy barrier is consistent with the experimental results, as we can directly observe the reaction in the Supporting Information STM Movies SM1 and SM2. There the reaction occurs at $T \sim 200$ K, where the 0.45−0.6 eV activation energy becomes available within a time scale comparable to the scanning rate. (In this estimate we use the Arrhenius equation with a prefactor of 10^{13} s^{-1}.)

Having identified the final reaction product, we now turn our attention to the reaction between an undissociated O_2 molecule and H_2O adsorbed on the anatase (101) surface. From our experiments we know that the O_2 molecules prefer adsorption in the vicinity of extrinsic defects[16] and typically remain undissociated even after annealing to room temperature. On the other hand, the experiment in Figure 1 clearly shows that the reaction with water results in terminal OH groups, which must involve O═O bond scission. The computed reaction pathway of an adsorbed O_2 molecule with H_2O is shown in Figure 4. This calculation was performed with 2 excess electrons in the slab (introduced either through two adsorbed H atoms on the back surface of the slab or via an adsorbed H plus a Nb impurity substituting a Ti atom, resulting in energetically similar defect states but at different locations in the slab, as shown in Supporting Information Figure SF3). When H_2O approaches the adsorbed peroxo O_2 molecule (Figure 4a), one proton is transferred, resulting in a terminal OH^- group and an OOH^- species:

$$(O_2)^{2-} + H_2O \rightarrow OH^- + OOH^- \quad (9)$$

This reaction provides a slight energy gain of 0.1 eV and is essentially barrierless (step i → ii in Figure 4a). The calculations indicate that the proton transfer only occurs when the O_2 molecule is in a peroxo state (the computed O═O bond length is 1.47 Å; note however that charge states in this work are only formal, as the electrons are partially delocalized and shared between the substrate and the adsorbed species). In the next step, the OOH^- can dissociate, resulting in another OH^- group and an $(O_2)_O$ molecule: see reaction ii→ v in Figure 4a.

$$OOH^- + O_s \rightarrow OH^- + (O_2)_O \quad (10)$$

The calculated activation barrier for the OOH^- dissociation in Figure 4a is quite large, 1.4 eV; see steps iii−v in Figure 4a. This is obviously overestimated in comparison to experiments, which show that the OOH^- decomposition can take place at room temperature, indicating that the activation barrier should actually be smaller than 1 eV. On the other hand, a relatively high activation barrier is consistent with IR absorption

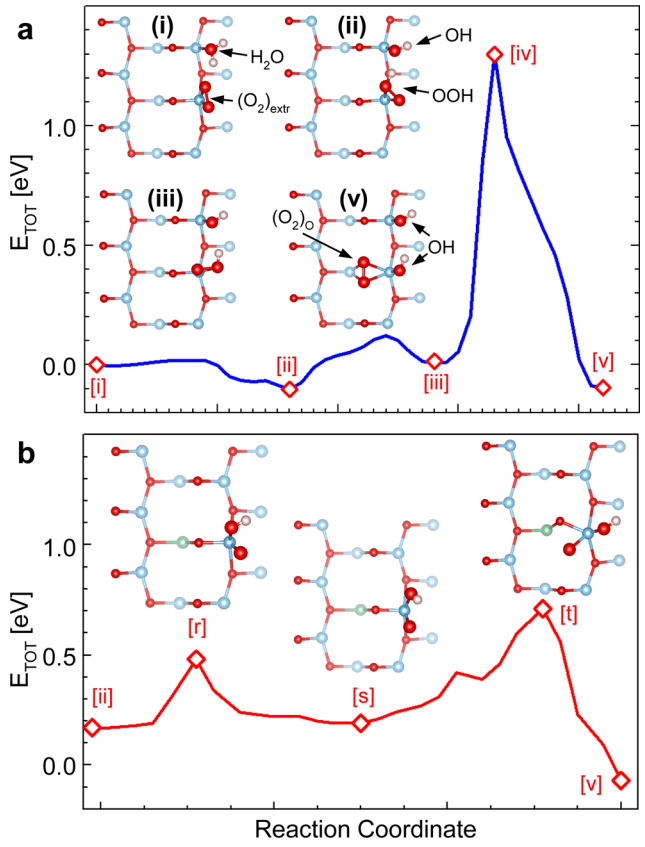

Figure 4. (a) Calculated NEB pathway for the reaction of H_2O with an adsorbed O_2 molecule (with 2 excess electrons in the slab, donated by H atoms). One proton is first transferred from H_2O to O_2, forming OH and OOH (step i → ii). The OOH group can consequently decompose into $(O_2)_O$ and another terminal OH group (step ii → v). (b) The NEB pathway for the step ii → v; here the excess electrons are donated to the slab by one Nb dopant and one H atom. Further, the terminal OH group originating from the first reaction step was removed from the slab.

studies,[32] which have identified OOH as metastable reaction intermediates in photocatalytic reactions.

To sort out the apparent discrepancy of the calculations with the experiment, we have investigated the activation barrier for the OOH^- dissociation in more detail. We found that the local availability of electrons is a critical factor. Excess electrons are required for weakening the O═O bond, while OOH^- has a relatively low affinity for electrons (compared to OH and O_2). The OOH group competes for electrons with other species adsorbed at the surface, notably with the OH group adsorbed right next to it in Figure 4a, and even with the H atoms at the backside of the slab, which are relatively deep donors.

The calculation for the OOH dissociation was repeated considering different surface configurations (see Figure SF4). In order to reduce the energy barrier for the OOH dissociation, the $(OH)^-$ group had to be removed from the slab, and one H dopant on the back surface was replaced by a substitutional Nb in proximity of the OOH (configuration in Figure SF5). In fact, we have previously found that the O_2 molecules prefer adsorption in the vicinity of these Nb dopants.[16] The pathway for the OOH dissociation in this slab is shown in Figure 4b. Here the OOH dissociates with an energy barrier of 0.5 eV (step ii → s). The resulting configuration in step s is further stabilized by transforming the O adatom into the final $(O_2)_O$

DOI: 10.1021/jacs.6b04004
J. Am. Chem. Soc. 2016, 138, 9565−9571

configuration, but there is an activation barrier of 0.7 eV for the process step s → v. We note that Nb-doped TiO_2 has been reported to be a good catalyst for ORR,[33] which is in-line with the calculations in Figure 4b.

In order to identify metastable reaction intermediates we tracked the reaction between the $(O_2)_{extr}$ and H_2O experimentally in Figure 5, at a lower temperature than in

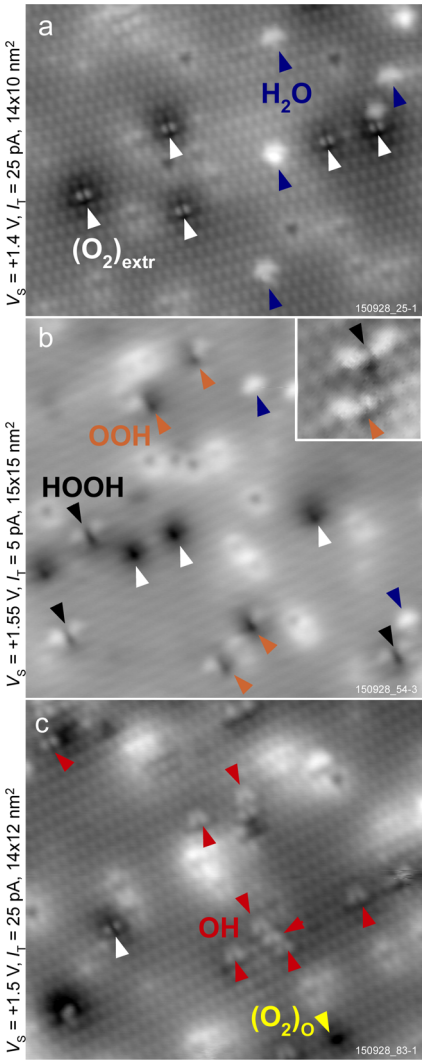

Figure 5. (a) H_2O and O_2 dosed in a 1:1 ratio at T < 60 K. (b) After annealing to 240 K. (c) After annealing to 300 K. White arrows mark $(O_2)_{extr}$ species, blue arrows H_2O molecules, orange OOH with a neighboring OH group, black arrows HOOH with two neighboring OH groups, red arrows mark terminal OH groups.

Figure 1. H_2O and O_2 were dosed in 1:1 ratio below 60 K, which results in single $(O_2)_{extr}$ species and H_2O molecules (marked by white and blue arrows, respectively, in Figure 5a). Figure 5b shows the surface after annealing to 240 K. Most of the H_2O molecules have disappeared, as they can diffuse across the surface and react with the adsorbed $(O_2)_{extr}$ species. New features appear in Figure 5b. Many of the original O_2 molecules have one or two flag-shaped features at the sides (marked by orange and black arrows, respectively). The inset in Figure 5b shows a detail of these species. We attribute the "one-flag" species (orange arrows) to the configuration calculated in Figure 4a(ii), where one hydrogen is transferred from the H_2O to the O_2, thus forming the OOH species and a terminal OH group nearby. This OH−OOH pair is kinetically frozen in this configuration, as the OH group cannot migrate away at this temperature, and the OOH species cannot decompose. We find the "flags" on either one or both sides of the $(O_2)_{extr}$ and take this as an indication that the formation of both species, OOH and HOOH, is possible. Our calculations show that HOOH is unstable in the presence of excess charge and spontaneously converts into two OH groups without any activation barrier (see Supporting Information Figure SF8). This is in contrast to the OOH species, which always require a significant activation energy for decomposition, even in the presence of excess electrons. This is in agreement with the experimental findings, which indicate that H_2O_2 is only stable when trapped between two terminal OH groups that either attract excess charge and/or geometrically prevent dissociation. The double-flag features marked by black arrows in Figure 5b are very unstable when imaged by STM. As a side, we note that the $(O_2)_{extr}$ species in Figure 5b are imaged only as a dark region, which is a reflection of the negative charge localized at the molecule. The difference from the typical $(O_2)_{extr}$ imaging (Figure 5a) originates from the low tunneling current of 5 pA. Higher tunneling currents decompose the double-flag feature. More details about the metastable species marked in Figure 5b are in Supporting Information Figure SF8.

After annealing to room temperature (Figure 5c), the metastable OOH and HOOH decompose, and we again find the terminal OH groups (marked by red arrows).

The results we have obtained on the anatase (101) surface are significantly different from the identical reaction on the rutile (110) surface.[11] The main difference is that the final reaction product between H_2O and O_2 on anatase (101) is the terminal OH group. For rutile, it was reported that terminal OHs recombine and desorb as H_2O at 300 K.[10] To investigate the macroscopic manifestation of the reaction between H_2O and O_2 on reduced anatase (101), we have measured TPD spectra (using $^{18}O_2$ with $D_2{}^{16}O$, see Figure 6). Panel a shows the desorption of $D_2{}^{16}O$ (mass 20), either as-adsorbed (black curve) or coadsorbed with $^{18}O_2$ (red curve). The intensity decreases, as some of the water desorbs as $D_2{}^{18}O$. The presence of $^{18}O_2$ also shifts the desorption temperature by 10 K. We attribute the slight shift of the desorption peak toward higher temperatures to weak attractive coupling between adsorbed D_2O and terminal OD groups. The shift of 10 K corresponds to ~20 meV attractive interaction.

The desorption of $D_2{}^{18}O$ is depicted in the red curve in panel b of Figure 6. This is the water that has reacted with the coadsorbed $^{18}O_2$, resulting in ^{18}OD groups that recombine. For completeness we also show the spurious $D_2{}^{18}O$ signal that results from scrambling on chamber walls as a black curve in panel a. The long tail toward higher temperature of the recombined water is consistent with the high thermal stability of the ^{18}OD observed in STM.

The charge state of the terminal OH groups is an important issue. In STM images, the anatase substrate around these species appears slightly darker, which is indicative of upward band bending.[34] The band bending induced by the adsorbed OH groups can be quantitatively estimated by XPS (from the core-level peak shift). The XPS spectra of Ti 2p and O 1s peaks are in the Supporting Information Figure SF9; the values of band bending measured during different stages of the terminal OH preparation are plotted in Figure 7. Dosing O_2 at 34 K and consequent annealing induced a band bending of 0.16 and 0.18

DOI: 10.1021/jacs.6b04004
J. Am. Chem. Soc. 2016, 138, 9565−9571

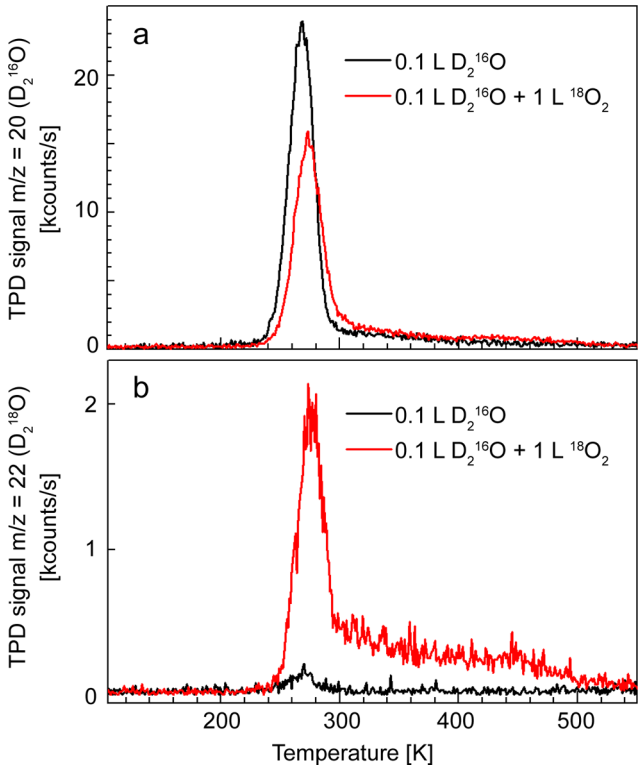

Figure 6. TPD spectra of the reaction between $^{18}O_2$ and $D_2{}^{16}O$: desorption of (a) $D_2{}^{16}O$ and (b) $D_2{}^{18}O$. The black curves are a reference, where only $D_2{}^{16}O$ was dosed. The red curves correspond to codosing of $^{18}O_2$ and $D_2{}^{16}O$.

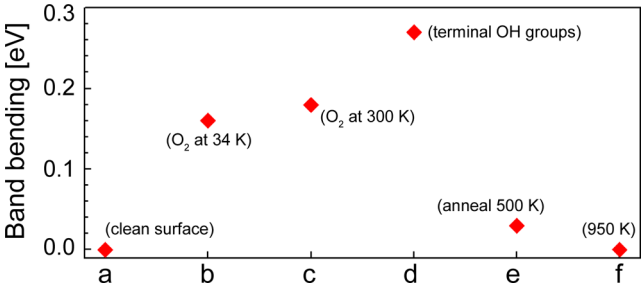

Figure 7. Upward band bending measured from the shift of core-level peaks in XPS during different stages of preparation of terminal OH groups: (a) clean surface, (b) dosing 1 ML O_2 at 34 K, (c) subsequent annealing to 300 K, (d) adding 1 ML H_2O and annealing to 300 K, which results in formation of terminal OH groups, (e) further annealing to 500 K, (f) annealing to 950 K.

eV, respectively (steps b and c). The surface was subsequently exposed to 1 ML of H_2O and annealed to 300 K (step d), which resulted in the formation of the terminal OH groups. Here the band bending further increased to 0.27 eV. Annealing this surface to 500 K (step e) resulted in desorption of most of the OH groups and the band bending decreased to 0.03 eV. Further annealing to 950 K (step f) removed the band bending completely.

DISCUSSION

It was reported that the rutile (110) surface exposed to H_2O and O_2 and annealed slightly above room temperature (340 K) contains mainly bridging OH groups.[11] This is in stark contrast to our observation of exclusively terminal OH on anatase (101). The calculated adsorption energies for these two species are given in Supporting Information Table ST2. The terminal OH group is ~0.2 eV more stable on anatase than on rutile, while the bridging OH group is ~1 eV more stable on rutile than on anatase. Our findings have several important consequences for photocatalysis: (1) The reaction between water and O_2 results in water dissociation, which does not occur spontaneously upon adsorption on the anatase (101) surface.[35] We note that the water dissociation is the step with the highest overpotential during photocatalytic water splitting.[36] (2) The terminal OH^- groups (also referred to as "basic hydroxyls") are negatively charged, which results in upward band bending at the surface.[34] The band bending is apparent in STM images and in core-level shifts in XPS data (Figure 7 and Supporting Information Figure SF9). The band bending creates an electric field in the near-surface region, and facilitates hole transfer toward the surface. We further note that the band bending induced by the terminal OH groups on anatase is opposite to the band bending induced by bridging OH groups on rutile ("acidic hydroxyls"). The surface chemistry of oxygen and water thus significantly affects band alignment between the two polymorphs.[37,38] (3) Terminal OH^- groups on anatase have a relatively high affinity to protons. Upon interaction with organic molecules, protons can be transferred from the molecule to the OH group, resulting in the formation of H_2O and a radical. This process plays an important role in activating organic molecules for photo-oxidation, and is likely important in water treatment applications. The importance of this step was studied for example in methanol photooxidation, where the methanol-to-methoxy transition cannot be directly achieved by a hole injection.[39,40] (4) The predominance of terminal OH^- groups on anatase observed in this work is consistent with the recent observation that anatase is the superior polymorph for photocatalytic production of free OH radicals.[41] (5) Our calculations indicate that the stability of the OOH intermediates is significantly affected by the presence of cationic (Nb^+) dopants in the near-surface region.

SUMMARY

We have shown that the reaction between water and oxygen on a reduced anatase (101) surface provides terminal OH groups, which are stable at room temperature. This behavior is significantly different from that of rutile. We have identified OOH as a metastable reaction product in the reaction. NEB calculations show that the energy barrier for OOH decomposition depends strongly on the local availability of excess electrons; in particular, the barrier is reduced to ~0.7 eV in the presence of subsurface Nb donors. The results reported here represent the electron-mediated ORR pathway but should also be relevant for the reverse reaction of photocatalytic water splitting. By showing the differences between rutile and anatase, and the role of a donor-type dopant, our work contributes to a better understanding of structure–reactivity relationships on oxide surfaces.

ASSOCIATED CONTENT

Supporting Information

The Supporting Information is available free of charge on the ACS Publications website at DOI: 10.1021/jacs.6b04004.

Details about the movie files; details regarding thermal stability, effect of dipole correction, energy levels and charge localization, OOH dissociation, stability of

DOI: 10.1021/jacs.6b04004
J. Am. Chem. Soc. 2016, 138, 9565–9571

hydroxyl groups, stability of HOOH in presence of excess charge, and additional measurements (PDF)
STM time-lapse movie of the reaction of $(O_2)_O$ with H_2O (AVI)
Movie similar to the preceding file but sample temperature was lowered to 200 K (AVI)
Calculated reaction pathway for eq 8: $(O_2)_O + H_2O \rightarrow 2OH + OS$ (AVI)
Calculated reaction pathway for an adsorbed O_2 molecule and H_2O (AVI)

AUTHOR INFORMATION

Corresponding Author

*setvin@iap.tuwien.ac.at

Notes

The authors declare no competing financial interest.

ACKNOWLEDGMENTS

The work was supported by the European Research Council (ERC) Advanced Grant "Oxide Surfaces" (ERC-2011-481 ADG_20110209) and by the Austrian Science Fund (FWF) project Wittgenstein Prize (Z 250 Wittgenstein-Preis). The work of A.S. and U.A. was supported by DoE-BES, Division of Chemical Sciences, Geosciences and Biosciences, under Award DE-FG02-12ER16286. We used computational resources of the National Energy Research Scientific Computing Center (DoE Contract No. DE-AC02-05CH11231) and the TIGRESS high performance computer center at Princeton University.

REFERENCES

(1) Linsebigler, A.; Lu, G.; Yates, J. T. *Chem. Rev.* **1995**, *95*, 735.
(2) Dohnalek, Z.; Lyubinetsky, I.; Rousseau, R. *Prog. Surf. Sci.* **2010**, *85*, 161.
(3) Thompson, T. L.; Yates, J. T. *Chem. Rev.* **2006**, *106*, 4428.
(4) Ni, M.; Leung, M. K. H.; Leung, D. Y. C.; Sumathy, K. *Renewable Sustainable Energy Rev.* **2007**, *11*, 401.
(5) Man, I. C.; Su, H. Y.; Calle-Vallejo, F.; Hansen, H. A.; Martinez, J. I.; Inoglu, N. G.; Kitchin, J.; Norskov, J. K.; Rossmeisl, J.; Jaramillo, T. F. *ChemCatChem* **2011**, *3*, 1159.
(6) Chen, J.; Li, Y.-F.; Sit, P.; Selloni, A. *J. Am. Chem. Soc.* **2013**, *135*, 18774.
(7) Wang, B. *J. Power Sources* **2005**, *152*, 1.
(8) Song, C.; Zhang, J. In *PEM Fuel Cell Electrocatalysts and Catalyst Layers*; Springer-Verlag: London, 2008; p 88.
(9) Dau, H.; Limberg, C.; Reier, T.; Risch, M.; Roggan, S.; Strasser, P. *ChemCatChem* **2010**, *2*, 724.
(10) Henderson, M. A.; Epling, W. S.; Peden, C. H. F.; Perkins, C. L. *J. Phys. Chem. B* **2003**, *107*, 534.
(11) Matthiesen, J.; Wendt, S.; Hansen, J.; Madsen, G. K. H.; Lira, E.; Galliker, P.; Vestergaard, E. K.; Schaub, R.; Laegsgaard, E.; Hammer, B.; Besenbacher, F. *ACS Nano* **2009**, *3*, 517.
(12) He, Y.; Dulub, O.; Cheng, H.; Selloni, A.; Diebold, U. *Phys. Rev. Lett.* **2009**, *102*, 106105.
(13) Scheiber, P.; Fidler, M.; Dulub, O.; Schmid, M.; Diebold, U.; Hou, W.; Aschauer, U.; Selloni, A. *Phys. Rev. Lett.* **2012**, *109*, 136103.
(14) Diebold, U. *Surf. Sci. Rep.* **2003**, *48*, 53.
(15) Du, Y.; Deskins, N. A.; Zhang, Z.; Dohnalek, Z.; Dupuis, M.; Lyubinetsky, I. *J. Phys. Chem. C* **2010**, *114*, 17080.
(16) Setvin, M.; Aschauer, U.; Scheiber, P.; Li, Y. F.; Hou, W.; Schmid, M.; Selloni, A.; Diebold, U. *Science* **2013**, *341*, 988.
(17) Setvin, M.; Daniel, B.; Mansfeldova, V.; Kavan, L.; Scheiber, P.; Fidler, M.; Schmid, M.; Diebold, U. *Surf. Sci.* **2014**, *626*, 61.
(18) Halwidl, D. *Development of an Effusive Molecular Beam Apparatus*; Springer Spektrum, 2016.
(19) Perdew, J. P.; Burke, K.; Ernzerhof, M. *Phys. Rev. Lett.* **1996**, *77*, 3865.
(20) Giannozzi, P.; Baroni, S.; Bonini, N.; Calandra, M.; Car, R.; Cavazzoni, C.; Ceresoli, D.; Chiarotti, G. L.; Cococcioni, M.; Dabo, I.; Dal Corso, A.; de Gironcoli, S.; Fabris, S.; Fratesi, G.; Gebauer, R.; Gerstmann, U.; Gougoussis, C.; Kokalj, A.; Lazzeri, M.; Martin-Samos, L.; Marzari, N.; Mauri, F.; Mazzarello, R.; Paolini, S.; Pasquarello, A.; Paulatto, L.; Sbraccia, C.; Scandolo, S.; Sclauzero, G.; Seitsonen, A. P.; Smogunov, A.; Umari, P.; Wentzcovitch, R. M. *J. Phys.: Condens. Matter* **2009**, *21*, 395502.
(21) Vanderbilt, D. *Phys. Rev. B: Condens. Matter Mater. Phys.* **1990**, *41*, 7892.
(22) Anisimov, V.; Zaanen, J.; Andersen, O. K. *Phys. Rev. B: Condens. Matter Mater. Phys.* **1991**, *44*, 943.
(23) De Angelis, F.; Di Valentin, C.; Fantacci, S.; Vittadini, A.; Selloni, A. *Chem. Rev.* **2014**, *114*, 9708.
(24) Henkelman, G.; Uberuaga, B. P.; Jonsson, H. *J. Chem. Phys.* **2000**, *113*, 9901.
(25) Setvin, M.; Daniel, B.; Aschauer, U.; Hou, W.; Li, Y.-F.; Schmid, M.; Selloni, A.; Diebold, U. *Phys. Chem. Chem. Phys.* **2014**, *16*, 21524.
(26) He, Y.; Tilocca, A.; Dulub, O.; Selloni, A.; Diebold, U. *Nat. Mater.* **2009**, *8*, 585.
(27) Herman, G. S.; Dohnalek, Z.; Ruzycki, N.; Diebold, U. *J. Phys. Chem. B* **2003**, *107*, 2788.
(28) Setvin, M.; Hao, X.; Daniel, B.; Pavelec, J.; Novotny, Z.; Parkinson, G. S.; Schmid, M.; Kresse, G.; Franchini, C.; Diebold, U. *Angew. Chem., Int. Ed.* **2014**, *53*, 4714.
(29) Pang, C. L.; Bikondoa, O.; Humphrey, D. S.; Papageorgiou, A. C.; Cabailh, G.; Ithnin, R.; Chen, Q.; Muryn, C. A.; Onishi, H.; Thornton, G. *Nanotechnology* **2006**, *17*, 5397.
(30) Wendt, S.; Matthiesen, J.; Schaub, R.; Vestergaard, E. K.; Laegsgaard, E.; Besenbacher, F.; Hammer, B. *Phys. Rev. Lett.* **2006**, *96*, 066107.
(31) Setvin, M.; Buchholz, M.; Hou, W.; Zhang, C.; Stöger, B.; Hulva, J.; Simschitz, T.; Shi, X.; Pavelec, J.; Parkinson, G. S.; Xu, M.; Wang, Y.; Schmid, M.; Wöll, C.; Selloni, A.; Diebold, U. *J. Phys. Chem. C* **2015**, *119*, 21044.
(32) Nakamura, R.; Nakato, Y. *J. Am. Chem. Soc.* **2004**, *126*, 1290.
(33) Arashi, T.; Seo, J.; Takanabe, K.; Kubota, J.; Domen, K. *Catal. Today* **2014**, *233*, 181.
(34) Ebert, P. *Surf. Sci. Rep.* **1999**, *33*, 121.
(35) He, Y.; Tilocca, A.; Dulub, O.; Selloni, A.; Diebold, U. *Nat. Mater.* **2009**, *8*, 585.
(36) Li, Y.-F.; Liu, Z.-P.; Liu, L.; Gao, W. *J. Am. Chem. Soc.* **2010**, *132*, 13008.
(37) Kavan, L.; Grätzel, M.; Gilbert, S. E.; Klemenz, C.; Scheel, H. J. *J. Am. Chem. Soc.* **1996**, *118*, 6716.
(38) Scanlon, D. O.; Dunnill, C. W.; Buckeridge, J.; Shevlin, S. A.; Logsdail, A. J.; Woodley, S. M.; Catlow, C. R. A.; Powell, M. J.; Palgrave, R. G.; Parkin, I. P.; Watson, G. W.; Keal, T. W.; Sherwood, P.; Walsh, A.; Sokol, A. A. *Nat. Mater.* **2013**, *12*, 798.
(39) Simschitz, T. *Surface Studies of Photocatalytic Reactions of Methanol on TiO_2 Anatase*; TU Wien: Vienna, 2015.
(40) Shen, M.; Henderson, M. A. *J. Phys. Chem. Lett.* **2011**, *2*, 2707.
(41) Odling, G.; Robertson, N. *ChemSusChem* **2015**, *8*, 1838.

DOI: 10.1021/jacs.6b04004
J. Am. Chem. Soc. 2016, 138, 9565−9571